Preparation of $AgInS_2$ nanocrystals and their application as sensitizers for TiO_2 nanorod array photoelectrodes

Jianbo Yin[1,3] and Junhong Jia[2]

[1]State Key Laboratory of Advanced Processing and Recycling of Non–ferrous Metals, Lanzhou University of Technology, Lanzhou 730050, P. R. China
[2]State Key Laboratory of Solid Lubrication, Lanzhou Institute of Chemical Physics, Chinese Academy of Sciences, Lanzhou 730000, P. R. China

E-mail: jianbery@163.com

Abstract. This paper reports the controlled synthesis of $AgInS_2$ nanocrystals and their application as sensitizers for TiO_2 nanorod array photoelectrode. The analytical results of high resolution transmission electron microscope (TEM) and laser particle analyzer show that the as–prepared $AgInS_2$ nanoparticles are highly crystallized with an average diameter of 16.67 nm. The results of ultraviolet (UV)–visible absorption spectra indicate that the as–prepared $AgInS_2$ nanoparticles have strong absorption in the spectral range of 300 nm–700 nm. The photovoltaic detectable results of TiO_2 nanorod array photoelectrode sensitized by $AgInS_2$ nanocrystals reveal that the composite films red shift to visible light range with high photovoltaic conversion efficiency of 2.076%, which is 3 times higher than that of bare TiO_2 photoelectrodes.

1. Introduction

In recent years, the controllable synthesis of nanostructural materials remains a research topic of great interest due to their unique chemical and physical properties and potential applications in various areas such as energy storage, luminescence and photoelectricity [1-3]. Metal sulfide nanostructural materials have attracted more and more researchers' attention due to their excellent luminescence and photoelectricity properties [4], for example, the excellent photoluminescence property of ZnS [5], the potential application of Cu_2S and CdS in photovoltaic fields [6, 7], and the appropriate band-gap of In_2S_3 and Bi_2S_3 [8-10]. Ternary metal sulfide semiconductors, alternatives for appropriate band–gap energies, have been the focus of much recent research because of their unique optical properties and electrical properties as well as their potential applications in linear and nonlinear optical devices and solar cells [11-14]. $CuInS_2$ with band gap energy of 1.50 eV and absorption coefficient 1.0×10^5 cm^{-1}, is considered to be ideal in solar cells [15-20]. However, few studies have been conducted on the photovoltaic characteristics of $AgInS_2$ so far, though its band gap energy is only 1.8 eV [21] and suitable for photovoltaic application. Yet, most researchers keep their eyes on the photocatalytic and luminescent properties. Tsuji and his coworkers reported photocatalytic characteristics of $AgInS_2$ and ZnS composite materials [22]; Torimoto and his partners studied their color–adjustable luminophore

[3] Address for correspondence: Jianbo Yin, to be contacted at State Key Laboratory of Recycling of Non–ferrous Metals, Lanzhou University of Technology, Lanzhou 730050, P. R. China. Tel.: +86 931 2973563; Fax: +86 931 2973563; E-mail: jianbery@163.com.

[23]; Hamanaka and his coworkers only studied the photoluminescence properties of $AgInS_2$ quantum dots [24], while ignored their photovoltaic characteristic; Cheng and his partners used $AgInS_2$ crystals as sensitizers on TiO_2 thin film solar cell, but only 0.05% low energy conversion efficiency was achieved [25].

In this paper, a high energy conversion efficiency of $AgInS_2$ nanocrystals as sensitizers is achieved and a systematic study of their photovoltaic application on TiO_2 nanorod arrays is discussed. The study results show that $AgInS_2$ nanocrystals are appropriate sensitizers.

2. Experimental

2.1. Chemicals

Indium (III) chloride tetrahydrate ($InCl_3 \cdot 4H_2O$), titanium tetrachloride ($TiCl_4$) and thiourea were purchased from Shanghai Chemical Reagent Corporation; thioglycolic acid, silver nitrate ($AgNO_3$), iodine, potassium iodide, hydrochloric acid, methanol anhydrous, ethanol absolute, hexane and acetonitrile were all obtained from Tianjin Chemical Reagent Corporation; Cetylamine (Chengdu) was purchased and used as–received.

2.2. Synthesis of $AgInS_2$ nanocrystals

Typical synthesis of $AgInS_2$ nanocrystals was shown as follows: $AgNO_3$ (1.0 mmol), $InCl_3 \cdot 4H_2O$ (1.0 mmol) and thiourea (2.0 mmol) were added to 20 mL cetylamine in a 50 mL three–necked bottle at 120ºC under the protection of N_2. After reaction for 5 minutes for nucleation, the system was subsequently heated to 180°C and the reaction continued for 60 minutes under N_2 flow. Cooling naturally, the nanocrystals were separated by adding 100 mL absolute ethanol. The nanocrystals were washed by excess absolute ethanol for two more times and dispersed in a methanol solution of thioglycollic acid (120 mM) and tetramethylammonium hydroxide (150 mM) to exchange cetylamine molecules which were adsorbent on the surface of nanocrystals for 60 minutes to activate the optical activity. After being precipitated with an ethyl acetate–hexane (1/4, v/v) solution, the as–prepared samples were redispersed in methanol.

2.3. Preparation of $AgInS_2$ nanocrystal sensitive solar cell

TiO_2 nanorod arrays were prepared on fluorine doped tin dioxide (FTO) substrates (20×20 mm) by hydrothermal route and the process was similar to the literature [26]. In order to attach the linker molecules to the TiO_2 surface, TiO_2 nanorod array film was immersed in acetonitrile solution of thioglycolic acid (1.2 M) and sulfuric acid (0.15 M) for 12 h. After that, spin–coating method was used for sensitized TiO_2 nanorod arrays by $AgInS_2$ nanocrystals for 2 times, 5 times and 10 times (1000 R/min), respectively. Then, I_2/KI solution with a definite concentration was used as the electrolyte, and transparent platinum glass electrode as the cathode to prepare $AgInS_2$ nanocrystal sensitive solar cell.

2.4. Characterization

High resolution transmission electron microscope (HRTEM, Hitach H–7500, Japan) was used to study the microstructure of the $AgInS_2$ nanocrystals, and the average diameter of the $AgInS_2$ nanocrystals was studied by laser particle size analyzer (Zetasizer Nano 3600). Scanning electron microscope (FESEM, JSM–6701F, Japan) was utilized to study the microstructure of the thin films. The crystal structure measurements of the samples were performed by power X–ray diffraction (XRD, Rigaku D/MAX–2500, Japan) using Cu Kα radiation (λ=0.15418 nm) at the scanning speed of 1.2°/min. UV–vis absorption spectra were recorded using a LabTech (China) spectrophotometer within the wavelength range of 300–1000 nm. The photovoltaic conversion efficiency of the sensitized TiO_2 arrays was studied by solar simulator of CELL–S500 (China).

3. Results and discussions

Figure 1 shows the morphology and structure characterization of TiO_2 nanorod array film. Figure 1a shows the general SEM image of TiO_2 nanorod arrays, and it can be seen that they are uniform on FTO from the inset of which the thickness is observed to be 1.0 μm. Seen from the TEM image (figure 1b), the average diameter of the nanorods is about 120 nm. Figure 1c reveals the clear lattice fringes of TiO_2 with an interplanar distance of about 0.323 nm, which is a typical characteristic fringe spacing of the (110) plane of rutile, showing that the TiO_2 nanorods grow along the (001) plane.

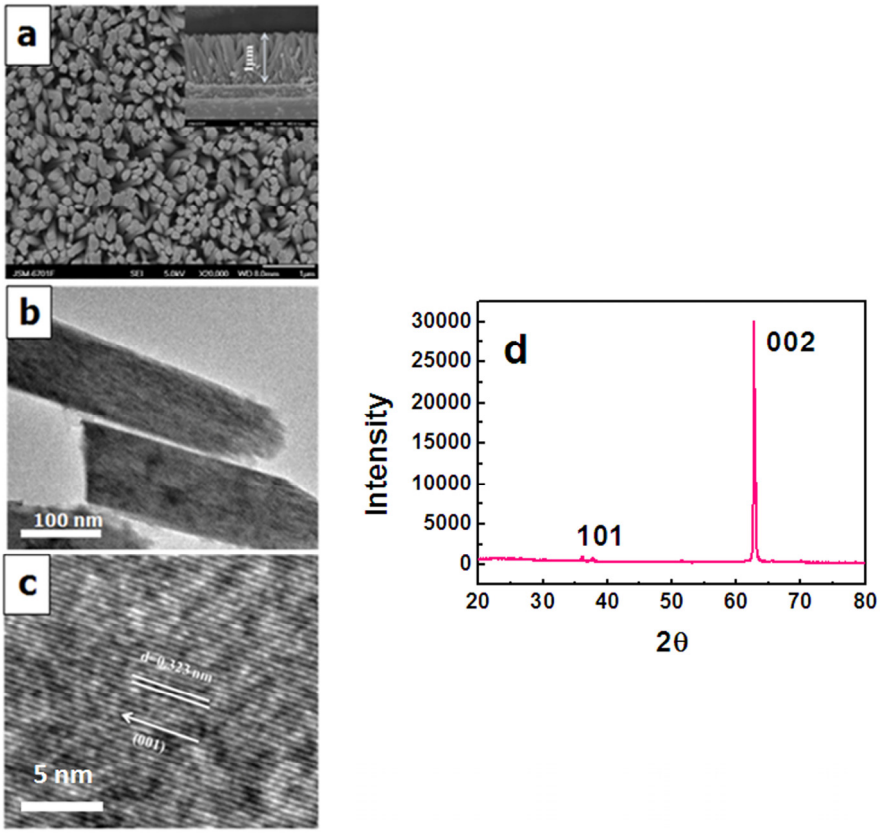

Figure 1. Characterization of TiO_2 arrays. (a) SEM image; (b) TEM image; (c) HRTEM; (d) XRD pattern.

Figure 1d displays the XRD patterns of TiO_2 nanorod arrays. All the diffraction peaks agree well with the tetragonal rutile phase (SG, P42/mmm; JCPDS No. 88–1175, a = b = 0.4517 nm and c = 0.2940 nm). Compared with the powder diffraction pattern, the (002) diffraction peak is significantly enhanced, and some diffraction peaks including (110), (111), and (211) are absent, which indicates that the nanorod arrays are highly oriented with respect to the substrate surface and the TiO_2 nanorods grow in the (001) direction with the growth axis parallel to the substrate surface. Moreover, these conclusions are also confirmed by HRTEM measurement.

Figure 2 shows characterization of $AgInS_2$ nanocrystals. Figure 2a displays the TEM image of monodispersed $AgInS_2$ nanocrystals with the average size range of 7–20 nm, which coincides with the characterization result of the laser particle size analyzer as shown in figure 2d where the average diameter is observed to be 16.67 nm. From the HRTEM image (figure 2b), it can be seen that these nanoparticles are well crystallized, and the inset of figure 3b reveals clear lattice fringes with an interplanar distance of about 0.356 nm which is a characteristic fringe spacing of the orthorhombic $AgInS_2$ crystal phase in the (120) crystal plane. The average particle size of the $AgInS_2$ nanocrystals is calculated to be about 16.5 nm according to Scherrer Equation which also matches the results of the

TEM and the laser particle size analyzer very well.

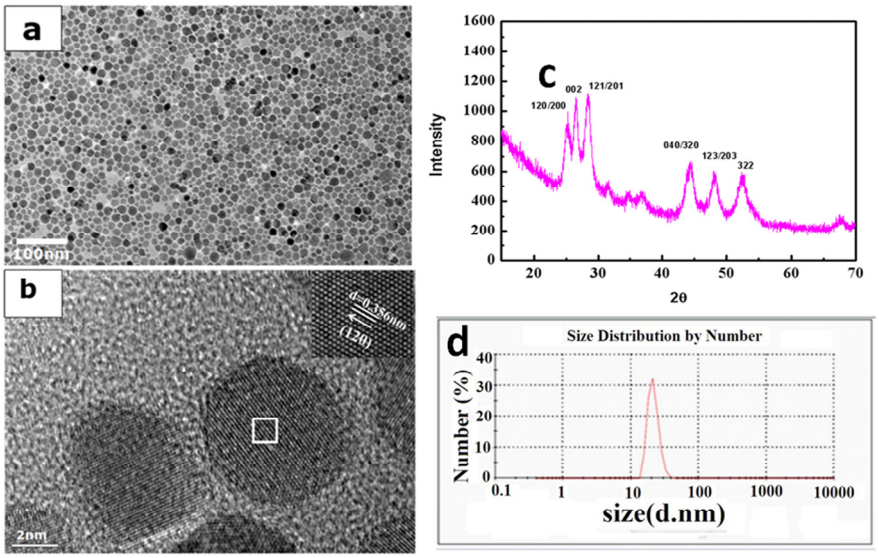

Figure 2. Characterization of $AgInS_2$ nanocrystals: (a) TEM image; (b) HRTEM image; (c) XRD pattern; (d) size distribution chart by number.

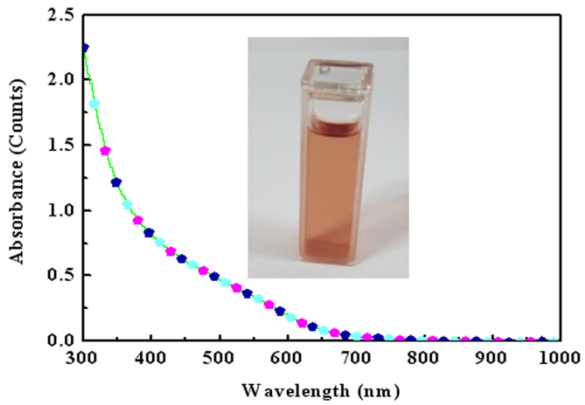

Figure 3. UV–vis absorption spectra of $AgInS_2$ nanocrystals.

The crystal structure of the as–synthesized products is examined by XRD. Figure 2c shows the XRD patterns of $AgInS_2$ nanocrystals, from which it can be seen that all the diffraction peaks can be assigned to the orthorhombic–phase $AgInS_2$, and this result has been also proven by the HRTEM (figure 2b).

The UV–vis absorption spectrum of $AgInS_2$ nanocrystals is shown in figure 3. It shows a wide absorption in the spectral range of 300 nm to 700 nm, and the wavelength of the absorption edge can be clearly identified at around 700 nm (corresponding to E_g of 1.8 eV). Since the E_g of $AgInS_2$ is reported to be 1.8 eV within the band energy range of 0.9–1.9 eV in which most of the solar energy can be absorbed, it can be one of the best solar cell sensitizers.

Figure 4 displays the SEM image of TiO_2 nanorod arrays sensitized by $AgInS_2$ nanocrystals for different spin–coating cycle times: 2, 5, and 10 times, respectively. The gap in the nanorod arrays is infilled slowly by $AgInS_2$ nanocrystals with the increase of spin–coating cycle times. After spin–coating for 2 times, few $AgInS_2$ nanocrystals can be observed under SEM (figure 4a), but after spin–coating for 10 times, very compact nanocomposite film is obtained, and the nanorod arrays can't be observed (figure 4c). The optimal spin-coating cycle is 5 times demonstrated by figures 4b and 5a and b, which indicates that they absorb a sufficient number of $AgInS_2$ nanocrystals with TiO_2 nanorod arrays being exposed on the surface. Figure 5c shows XRD patterns of the TiO_2 nanorod arrays

sensitized by $AgInS_2$ nanocrystals. All the diffraction peaks can be attributed to the tetragonal rutile phase TiO_2 and orthorhombic $AgInS_2$ crystals. The peak in (002) plane is weakening compared with figure 1b because it is covered by $AgInS_2$ crystals. The peaks in (121), (040) and (323) crystal planes show that the $AgInS_2$ nanocrystals have no remarkable change.

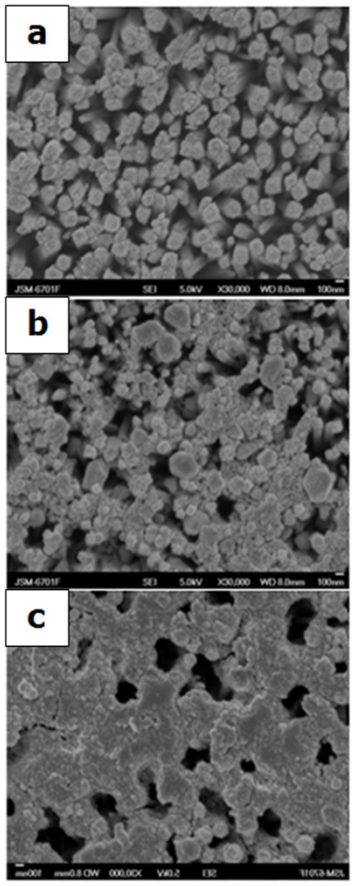

Figure 4. FESEM images of TiO_2 nanorod arrays for different spin–coating times. (a) for 2 times; (b) for for 5 times. (c) for 10 times.

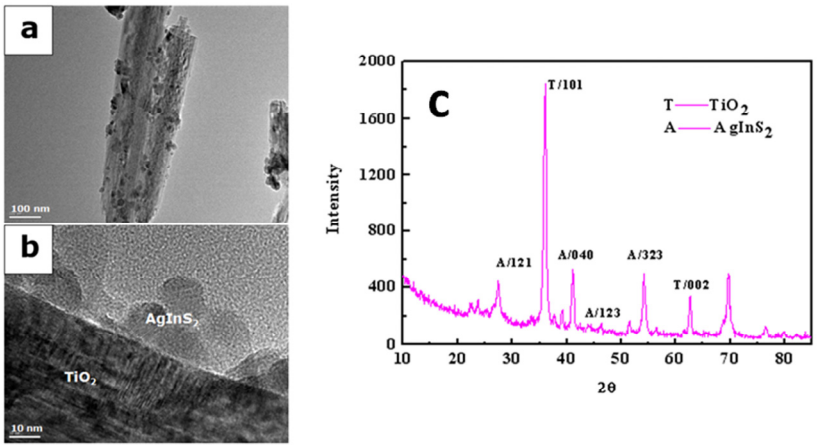

Figure 5. TEM images of TiO_2 nanorod arrays sensitized by $AgInS_2$ nanocrystals spin–coating for 5 times. (a) general image; (b) detailed image; (c) XRD pattern.

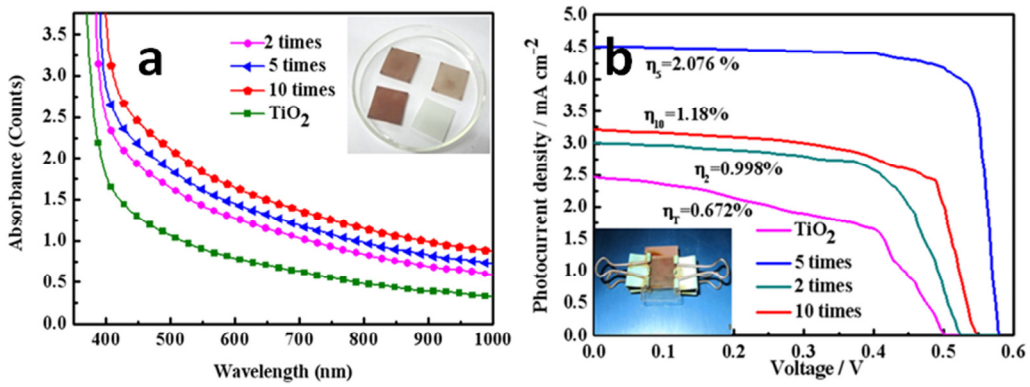

Figure 6. (a) UV–vis absorption spectra of TiO_2 nanorod arrays sensitized by $AgInS_2$ crystals; (b) the photocurrent density–voltage (J–V) curves of the TiO_2 solar cells sensitized by $AgInS_2$ nanocrystals for different spin–coating times under AM 1.5 illumination of 100 mW cm^{-2}.

The UV–vis absorption spectra of TiO_2 nanorod arrays sensitized by $AgInS_2$ nanocrystals are shown in figure 6a. It can be seen that the optical absorption of the TiO_2 nanorod arrays is in the ultraviolet region. However, after being sensitized by $AgInS_2$ nanocrystals, the absorption edges of the thin films can red shift to the visible region, and the red shift length increases with the sensitized times, indicating that $AgInS_2$ nanocrystals as the sensitizers for TiO_2 nanorod arrays expand the photoabsorption range.

Figure 6b shows the photocurrent density–voltage (J–V) curves of the solar cells based on the TiO_2 photoelectrodes sensitized by $AgInS_2$ nanocrystals with an active area of about 0.78 cm^2 under AM 1.5 illumination of 100 mW cm^{-2} for 20 times cycles. The photovoltaic parameters of the solar cells are summarized in table 1. It shows that the solar cell based on bare TiO_2 indicates a short–circuit photocurrent density (Jsc) of 2.474 mA cm^{-2}, an open–circuit voltage of 501 mV, a fill factor (FF) of 59.5%, and a conversion efficiency of 0.672%. The relatively low efficiency is ascribed to the low density uniform TiO_2 nanorod arrays thin film, which decreases the surface area and the effective quantity of the photo–generated electrons. The relatively high efficiency of thin film can be attributed to the sensitizers $AgInS_2$ nanocrystals on the surface of TiO_2 nanorods that absorb more solar energy and generate more photo–generated electrons than bare TiO_2 as shown in table 1 (Cell 2 and Cell 3). After being sensitized for 2 times, the energy conversion efficiency is 1.18%, and it almost improves twice up to 2.076% after being sensitized for 5 times and the FF is 70.8% which is the max one of all the values shown in table 1. The decrease of conversion efficiency of Cell 4 is due to a large amount of $AgInS_2$ nanocrystals being deposited on the TiO_2 film, which agglomerate into chunks and lead to a decrease of quantum efficiency.

Table 1. Photovoltaic parameters of the TiO_2 solar cells sensitized by $AgInS_2$ nanocrystals for different spin–coating times: 2 times (TiO_2–2), 5 times (TiO_2–5) and 10 times (TiO_2–10) under AM 1.5 illumination of 100 mW cm^{-2}.

Sample	Sensitized times	V_{oc} (mV)	J_{sc} (mA cm^{-2})	FF (%)	η (%)
Cell 1	0	501	2.474	59.5	0.672
Cell 2	2	546	3.218	67.1	0.998
Cell 3	5	576	4.513	70.8	2.076
Cell 4	10	525	3.013	65.4	1.180

4. Conclusion

Orthorhombic $AgInS_2$ nanocrystals are synthesized by a simple wet chemical route. The results of TEM and laser particle size analyzer show that the diameter of the $AgInS_2$ nanocrystals is 16.67 nm; and they have strong optical absorption in the spectral range of 300 nm–700 nm. The study results show that $AgInS_2$ nanocrystals are suitable for use as sensitizers for solar cells. The sensitized results show that the max energy conversion efficiency is 2.076 % after spin–coating for 5 times, and after that the energy conversion efficiency decreases with the increasing the spin–coating times.

References

[1] Bondarev V A 1997 Variational method for solving non-linear problems of unsteady-state heat conduction *Int. J. Heat Mass Transf.* **40** 3487
[2] Zhu J, Li Q, Bi W, et al. 2013 Ultra–rapid microwave–assisted synthesis of layered bultrath in birnessite $K_{0.17}MnO_2$ nanosheets for efficient energy storage *J. Mater. Chem. A.* **1** 8154-9
[3] Mishra S, Rajeswari R, Vijayan N, et al. 2013 Probing the structure, morphology and multifold blue absorption of a new red–emitting nanophosphor for LEDs *J. Mater. Chem. C.* **1** 5849-55
[4] Zhu Y P, Ren T Z and Yuan Z Y 2014 Mesoporous non–siliceous inorganic–organic hybrids: A promising platform for designing multifunctional materials *New J. Chem.* **38** 1905-22
[5] Mao B, Chuang C H, McCleese C, et al. 2014 Near–infrared emitting $AgInS_2$/ZnS nanocrystals *J.*

Phys. Chem. C. **118** 13883-9
[6] Zhu Y P, Li J, Ma T Y, et al. 2014 Sonochemistry–assisted synthesis and optical properties of mesoporous ZnS nanomaterials *J. Mater. Chem. A.* **2** 1093-101
[7] Zhu G, Pan L, T. Xu, et al. 2011 One–step synthesis of CdS sensitized TiO_2 photoanodes for quantum dot–sensitized solar cells by microwave assisted chemical bath deposition method *ACS Appl. Mater. Interf.* **3** 1472-8
[8] Palacios P, Aguilera P, Wahnon I, et al. 2009 Simple and generalized synthesis of semiconducting metal sulfide nanocrystals *Adv. Function. Mater.* **19** 1645-9
[9] Ye F, Wang C, Du G, et al. 2011 Large–scale synthesis of In_2S_3 nanosheets and their rechargeable lithium–ion battery *J. Mater. Chem.* **21** 17063-5
[10] Heeá Kim Y, Haká Lee J, Miná Park S, et al. 2010 Synthesis of shape–controlled β–In_2S_3 nanotubes through oriented attachment of nanoparticles *Chem. Commun.* **46** 2292-4
[11] Wu T, Zhou X, Zhang H, et al. 2010 Bi_2S_3 nanostructures: a new photocatalyst *Nano Research* **3** 379-86
[12] Chang S H, Chiu B C, Gao T L, et al. 2014 Selective synthesis of copper gallium sulfide ($CuGaS_2$) nanostructures of different sizes, crystal phases, and morphologies *Cryst. Eng. Comm.* 16 3323-30
[13] Yin J and Jia J 2014 Synthesis of Cu_3BiS_3 nanosheet films on TiO_2 nanorod arrays by a solvothermal route and their photoelectrochemical characteristics *Cryst. Eng. Comm.* **16** 2795-801
[14] Lin Z, Fei X and Ma Q 2014 $CuInS_2$ quantum dots@silica near–infrared fluorescent nanoprobe for cell imaging *New J. Chem.* **38** 90-6
[15] Yang F, Kuznietsov V and Lublow M 2013 Solution synthesis of high–quality $CuInS_2$ quantum dots as sensitizers for TiO_2 photoelectrodes *J. Mater. Chem. A.* **1** 6407-15
[16] Tang Y, Ng Y H, Yun J H, et al. 2014 Fabrication of a $CuInS_2$ photoelectrode using a single–step electrodeposition with controlled calcination atmosphere *RSC Adv.* **4** 3278-83
[17] Li Q, Zhai L, Zou C, et al. 2013 Wurtzite $CuInS_2$ and $CuIn_xGa_{1-x}S_2$ nanoribbons: Synthesis, optical and photoelectrical properties *Nanoscale* **5** 1638-48
[18] Guo K, Liu Z, Han J, et al. 2014 Hierarchical TiO_2–$CuInS_2$ core–shell nanoarrays for photoelectrochemical water splitting *Phys. Chem. Chem. Phys.* **16** 16204-13
[19] Yang J, Bao C, Zhang J, et al. 2013 In situ grown vertically oriented $CuInS_2$ nanosheets and their high catalytic activity as counter electrodes in dye–sensitized solar cells *Chem. Commun.* **49** 2028-30
[20] Gunawan, Septina W and Ikedal S, et al. 2014 Platinum and indium sulfide–modified $CuInS_2$ as efficient photocathodes for photoelectrochemical water splitting *Chem. Commun.* **50** 8941-3
[21] Cheng K W and Wang S C 2009 Effects of complex agents on the physical properties of Ag–In–S ternary semiconductor films using chemical bath deposition *Mater. Chem. Phys.* **115** 14-20
[22] Tsuji I, Kato H, Kobayashi H, et al. 2004 Photocatalytic H_2 evolution reaction from aqueous solutions over band structure–controlled (AgIn)xZn_2(1–x)S_2 solid solution photocatalysts with visible–light response and their surface nanostructures *J. Am. Chem. Soc.* **126** 13406-13
[23] Torimoto T, Adachi T, Okazaki K, et al. 2007 Facile synthesis of ZnS–$AgInS_2$ solid solution nanoparticles for a color–adjustable luminophore *J. Am. Chem. Soc.* **129** 12388-9
[24] Hamanaka Y, Ogawa T and Tsuzuki M 2011 Photoluminescence properties and its origin of $AgInS_2$ quantum dots with chalcopyrite structure *J. Phys. Chem. C* **115** 1786-92
[25] Cheng K, Law W C, Yong K T, et al. 2011 Synthesis of near–infrared silver–indium–sulfide ($AgInS_2$) quantum dots as heavy–metal free photosensitizer for solar cell applications *Chem. Phys. Lett.* **515** 254-7
[26] Liu B and Aydil E S 2009 Growth of oriented single–crystalline rutile TiO_2 nanorods on transparent conducting substrates for dye–sensitized solar cells *J. Am. Chem. Soc.* **131** 3985-90